Ultrasensitive nonlinear vibrational spectroscopy of complex molecular systems

Selig, O.

[Link to publication](#)

CHAPTER 2

THEORY

2.1 MACROSCOPIC ELECTRODYNAMICS

2.1.1 MAXWELL'S EQUATIONS

The basis for describing electric and magnetic fields and their interaction with matter is given by Maxwell's equations, which were published by their namesake James Clerk Maxwell in 1861. In 1884 Oliver Heaviside reformulated the equations to their nowadays well-known form. The macroscopic Maxwell equations in their differential form in SI units read (e.g.[40]):

$$\nabla \cdot \vec{D}(\vec{r}, t) = \rho(\vec{r}, t) \tag{2.1a}$$

$$\nabla \cdot \vec{B}(\vec{r}, t) = 0 \tag{2.1b}$$

$$\nabla \times \vec{E}(\vec{r}, t) = -\frac{\partial \vec{B}(\vec{r}, t)}{\partial t} \tag{2.1c}$$

$$\nabla \times \vec{H}(\vec{r}, t) = \frac{\partial \vec{D}(\vec{r}, t)}{\partial t} + \vec{j}(\vec{r}, t), \tag{2.1d}$$

where $\vec{j}$ and ρ are the current and charge densities, $\vec{E}$ is the electric field, $\vec{D}$ the electric displacement, $\vec{H}$ the magnetic field and $\vec{B}$ the magnetic induction. Since the materials investigated in this thesis are nonmagnetic ($\mu_r = 1$), we will focus on describing the interaction of matter with the electric field. The presence of an external electric field can induce electric dipoles $\vec{\mu}$ inside the volume V of medium resulting in a macroscopic polarization $\vec{P}(\vec{r}, t) = 1/V \sum_{i=1}^{n} \vec{\mu}_i(\vec{r}, t)$. If the applied electric field strength is small, the polarization increases linearly with the field:

$$\vec{P} = \varepsilon_0 \chi_e \vec{E}, \tag{2.2}$$

where χ_e is the electric susceptibility. For a monochromatic electric field, the electric displacement field inside a material is given by:

$$\vec{D} = \varepsilon_0 \vec{E} + \vec{P} = (1 + \chi_e)\varepsilon_0 \vec{E} = \varepsilon_r \varepsilon_0 \vec{E}, \tag{2.3}$$
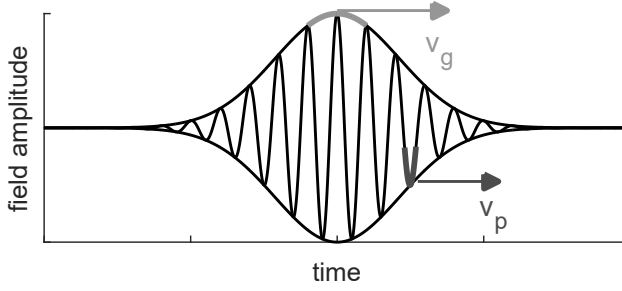
FIGURE 2.1. Field amplitude of a propagating (polychromatic) light pulse with indicated group (v_g) and phase velocity (v_p).

where ε_0 is the vacuum permittivity. From the last equation follows that the displacement field also increases linearly with the electric field where ε_r, the material permittivity, is the proportionality constant. It is worth noting that χ_e and ε_r are complex tensors in general and only reduce to scalars for isotropic media and small electric field strengths.

The propagation of electromagnetic fields is described by the wave equation which can be derived by taking the curl of Eq. (2.1c), assuming a source-free medium ($\rho = 0$, $\vec{j} = 0$), and making use of Eq. (2.1d) and Eq. (2.3):

$$\left(\nabla^2 - \frac{1}{c^2}\frac{\partial^2}{\partial t^2}\right)\vec{E} = \mu_0 \frac{\partial^2}{\partial t^2}\vec{P},\tag{2.4}$$

where $c = \sqrt{(\varepsilon_0\mu_0)^{-1}}$ is the speed of light in vacuum, and μ_0 the vacuum permeability.

2.1.2   THE REFRACTIVE INDEX n

To describe the propagation of light inside a material it is convenient to introduce the material specific refractive index. By assuming a nonmagnetic material $\mu_r = 1$ we can relate the refractive index n, the dielectric function, and the susceptibility via:

$$n = \sqrt{\varepsilon_r \mu_r} \approx \sqrt{1 + \chi} = \tilde{n} + i\kappa.\tag{2.5}$$

In the last equation we have written the refractive index as sum of the real ($\tilde{n}$) and imaginary (κ) part of n. To understand the properties of the refractive index, it is insightful to investigate the implication for a monochromatic plane wave with frequency ω traveling through the material:

$$E = E_0 e^{i(kx - \omega t)} + c.c..\tag{2.6}$$

Here k denotes the wave vector, and $c.c.$ refers to the complex conjugate. The wave vector is defined as[41]

$$k = \frac{n(\omega)\omega}{c}\tag{2.7}$$

and is in general complex valued due to its dependence on $n(\omega)$. Combining the last two equations leads to:

$$E = E_0 e^{i\omega(\frac{\tilde{n}}{c}x - t)} \cdot e^{-\omega\frac{\kappa}{c}x} + c.c., \tag{2.8}$$

where we have separated the exponent into an oscillating contribution depending on $\tilde{n}$ and an exponentially decaying contribution depending on κ. Thus, a nonvanishing imaginary part of n leads to a decrease of the amplitude as the wave travels through the medium. We can quantify the amount of attenuation by inspecting the light intensity of a plane wave inside the material, which is given by:[42]

$$I = \frac{1}{2}c\sqrt{\varepsilon_r}\mathscr{R}e\{E \cdot E^*\} = \frac{1}{2}c\sqrt{\varepsilon_r}e^{-2\omega\frac{\kappa}{c}x}|E_0^2|, \tag{2.9}$$

where the asterisk denotes the complex conjugate. By comparing the last equation to the Lambert-Beer law:

$$I = I_0 e^{-\alpha x}, \tag{2.10}$$

we see that the absorption coefficient α is related to the imaginary part of the refractive index by:

$$\alpha = 2\frac{\kappa}{c}\omega. \tag{2.11}$$

Next, we look at the influence of the real part of the refractive index $\tilde{n}$ on the oscillating part of the electric field which governs the velocity of the wave. Monochromatic plane waves (see Eq. (2.8)) propagate at the phase velocity:

$$v_p(\omega) = \frac{c}{\tilde{n}(\omega)} \tag{2.12}$$

through the medium. Therefore, the real part of the refractive index determines the speed of light inside a material (relative to the speed of light in vacuum). If $\tilde{n}$ is frequency dependent ($\frac{\partial \tilde{n}}{\partial \omega} \neq 0$), then the medium is often referred to be dispersive. In this thesis we employ ultrashort light pulses, consisting of multiple frequency components, to study the molecular dynamics of bulk samples. The envelope of the light pulses, will travel at a constant group velocity:[41]

$$v_g = \frac{c}{\tilde{n} + \omega\frac{d\tilde{n}}{d\omega}}. \tag{2.13}$$

If the group velocity is also frequency dependent, then the pulse will spread with propagation time. Figure 2.2 shows the real and imaginary part of the refractive index close to a resonance. The lineshape of the real part extends over a much broader frequency region than the imaginary part, which implies that severe pulse elongation can occur even though the medium is transparent ($\kappa \approx 0$).

2.1.3 MODELS FOR THE REFRACTIVE INDEX

To describe the frequency dependence of the refractive index, we assume that an electric field $\vec{E} = \vec{E}_0 e^{-i\omega t}$ inside a material can displace charges, like electrons,
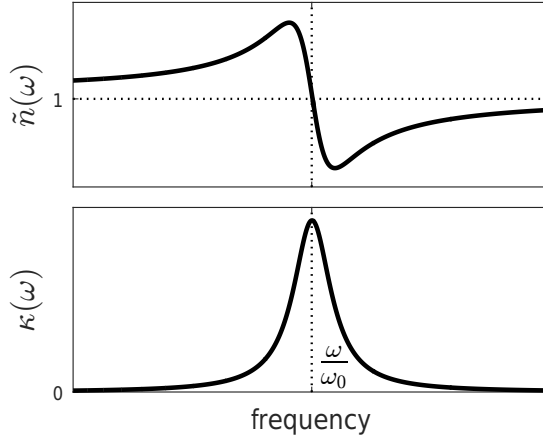
FIGURE 2.2. Frequency dependence of the real $\tilde{n}$ and imaginary κ part of the refractive index n in vicinity of a resonance at ω_0.

ions[43].[44] For small electric field strengths the bound charges with effective mass m and charge q will experience a restoring force with spring constant k. In addition, the movement of the charges will be damped by a general friction term Γ due to, among others, radiative damping.[42] Summing over all presented terms allows us to write the equation of motion:

$$m\frac{\partial^2 \vec{x}}{\partial t^2} = F_{restore} + F_{damp} + F_{drive} \tag{2.14}$$

$$= -k\vec{x} - m\Gamma\frac{\partial \vec{x}}{\partial t} + q\vec{E}_0 e^{-i\omega t}. \tag{2.15}$$

This differential equation can be solved by using the ansatz $\vec{x} = \vec{x}_0 e^{-i\omega t}$ which leads to:

$$\vec{x}_0 = \frac{q\vec{E}_0}{m} \cdot \frac{1}{\omega_0^2 - \omega^2 - i\Gamma\omega}, \tag{2.16}$$

where we have introduced the fundamental frequency $\omega_0 = \sqrt{\frac{k}{m}}$ of the oscillator. Since the oscillators inside the medium can have different properties (like friction terms), and experience different local environments, we can divide them into ensembles i with the oscillator densities N_i, local friction terms Γ_i and fundamental frequencies ω_i. By combining the expression for the displacement of the charge $\vec{x}$, with the definition for the microscopic dipole $\vec{\mu} = q\vec{x}$ and Eq. (2.3) we can express the dielectric function as:

$$\varepsilon_r(\omega) = 1 + \sum_i \frac{q^2}{m_i \varepsilon_0} \frac{N_i}{\omega_i^2 - \omega^2 - i\Gamma_i\omega}. \tag{2.17}$$

Figure 2.2 shows the dielectric function close to a resonance.
Equation 2.17 (Lorentz model[42]) provides a general approach for charge displacement
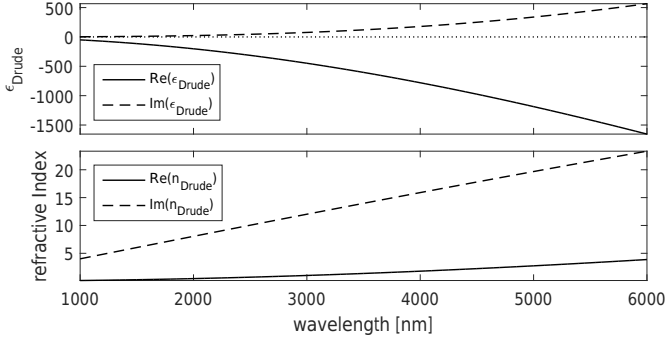
FIGURE 2.3. Dielectric function (top) and refractive index (bottom) of gold calculated with the Drude model ($\Gamma = 17.1 \cdot 10^{12}$ s^{-1}, $\omega_p = 2.15 \cdot 10^{15}$ s^{-1}[46]).

and offers an accurate description for a wide range of phenomena including bound electrons, dielectrics and molecular vibrations.

For (noble) metals at visible and infrared frequencies where the majority of the accessible charges originate from free electrons, the Lorentz model reduces to the Drude model.[45] In this special case, the restoring force vanishes ($k = 0$) and we can substitute the electron mass m_e, charge $q = -e$ and density n into Eq. (2.17) and arrive at:

$$\varepsilon_r(\omega) = 1 + \frac{e^2 n}{m_e \varepsilon_0} \frac{1}{-\omega^2 - i\Gamma\omega} = 1 - \frac{\omega_p^2}{\omega^2 + i\Gamma\omega}, \tag{2.18}$$

where we have introduced the material specific plasma frequency $\omega_p = \sqrt{\frac{e^2 n}{m_e \varepsilon_0}}$.

Figure 2.3 shows the real and imaginary part of the dielectric function of gold calculated with literature values for Γ and ω_p.[46] With increasing wavelength the real part of ε_r decreases monotonically and the imaginary part increases monotonically. The Drude model reproduces the experimental data of noble metals, like gold, very well in the infrared, but it breaks down in the visible and ultraviolet frequency range where interband transition from bound electrons becomes a dominant contribution to the dielectric function.[47]

Since for most metals the friction term is significantly smaller than the plasma frequency ($\Gamma \ll \omega_p$), the dielectric function can be further simplified to:

$$\varepsilon_r \approx 1 - \frac{\omega_p^2}{\omega^2}. \tag{2.19}$$

Using the Fresnel equation to determine the reflectivity, one can show that materials with a negative real part act as good reflectors. However, for $\omega > \omega_p$ ε_r becomes positive and the material becomes transparent.[41] The plasma frequency of most metals is in the ultraviolet, explaining why they are good mirrors in the visible and the infrared.
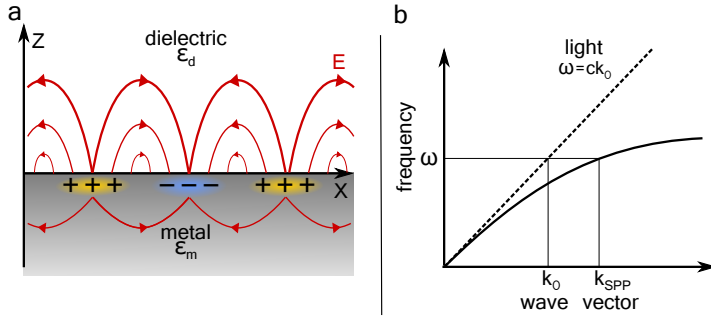
FIGURE 2.4. a) Charge density and electric field of a surface-plasmon-polariton (SPP) at the metal-dielectric interface. b) Dispersion relation of a plane wave in vacuum (dashed) and a SPP (straight).

2.2 PLASMONICS

Plasmonic nanoantennas have the ability to localize energy from the free radiation field to their direct vicinity (see Fig. 2.6). In Chapter 5 and Chapter 6 we will show how the near-field enhancement associated with this process can be exploited to greatly increase the signals in nonlinear infrared spectroscopy.

The following section will provide some theoretical background. We will first introduce the surface-plasmon-polariton as a solution to Maxwell's equations at the plane metal-dielectric interface. In the second part we will make the connection with nanoantennas by considering sub-wavelength particles. Nanoantennas can be resonantly driven by the external light field leading to strongly localized particle-plasmon-polaritons (PPP). We will introduce two intuitive models to explain the origin of the resonance condition of the PPPs and show how it is affected by the antenna geometry.

2.2.1 SURFACE PLASMON POLARITONS

Figure 2.4a shows a schematic representation of a surface-plasmon-polariton (SPP) which is the charge density oscillation and the accompanying electromagnetic wave at the interface of a dielectric and a material with (close to) free electrons, like most noble metals.[48]

To show that SPPs are solutions of Maxwell's equations it is sufficient to look at a two dimensional system (x-z-plane) where the dielectric and the metal form an interface along the x-axis, and the materials have respective dielectric constants ε_d and ε_m. Here we assume that both dielectric constants are real. We will use a p-polarized wave which propagates along the x-axis in the x-y-plane and has wave vector components parallel $k_{\parallel}$ and perpendicular $k_{\perp}$ to the interface. Since SPPs are bound to the interface, the electric field has to decay exponentially into both media. Therefore, the perpendicular component of the wave vector $k_{\perp}$ has to be imaginary. We are assuming that the plasmon propagates along the interface (x-direction). Therefore,

the wave vector component parallel to the interface $k_\parallel$ has to have a real part. Hence, the electric field inside the metal (m) and dielectric (d) are given by:

$$\vec{E}_l = \begin{pmatrix} E_\parallel \\ 0 \\ E_\perp \end{pmatrix} e^{i(k_{\parallel,l}x - \omega t)} e^{ik_{\perp,l}z} \quad l = m,d. \tag{2.20}$$

Because we consider a material without any excess charge carriers, $\nabla \cdot \vec{D} = 0$ we find that

$$k_{\parallel,l} E_{\parallel,l} + k_{\perp,l} E_{\perp,l} = 0 \quad l = m,d. \tag{2.21}$$

Next we use the standard electromagnetic boundary conditions at a charge-free interface:[40]

$$E_{\parallel,m} - E_{\parallel,d} = 0 \tag{2.22}$$

$$\varepsilon_m E_{\perp,m} - \varepsilon_d E_{\perp,d} = 0. \tag{2.23}$$

The last four equations only have a nontrivial solution for

$$\varepsilon_m k_{\perp,d} - \varepsilon_d k_{\perp,m} = 0. \tag{2.24}$$

Lastly, we use the dispersion relation of a homogeneous medium:[40, 41]

$$\varepsilon_l k^2 = k_{\perp,l}^2 + k_{\parallel,l}^2 \quad l = d,m, \tag{2.25}$$

where k is the wave vector in vacuum. Combining Eq. (2.24) and Eq 2.25, and using the fact that the parallel component of the wave vector has to be conserved,[41] we find for the components of the wave vector:

$$k_\parallel = \sqrt{\frac{\varepsilon_m \varepsilon_d}{\varepsilon_m + \varepsilon_d}} \frac{\omega}{c} \tag{2.26}$$

$$k_{\perp,l} = \sqrt{\frac{\varepsilon_l^2}{\varepsilon_m + \varepsilon_d}} \frac{\omega}{c} \quad l = m,d. \tag{2.27}$$

Electric fields that are confined to an interface decay exponentially into both media. Therefore, it follows from Eq. (2.27) that the sum of the dielectric functions has to be negative. Demanding a real solution for $k_\parallel$ also requires the product of the dielectric functions to be negative, therefore:

$$\varepsilon_d \cdot \varepsilon_m < 0 \tag{2.28}$$

$$\varepsilon_d + \varepsilon_m < 0. \tag{2.29}$$

It is easy to find material pairs that fulfil these requirements. As was shown in Section 2.1.3, the dielectric function of noble metals is mainly composed of a large, negative real part at visible and infrared frequencies, and dielectrics like air, glass or
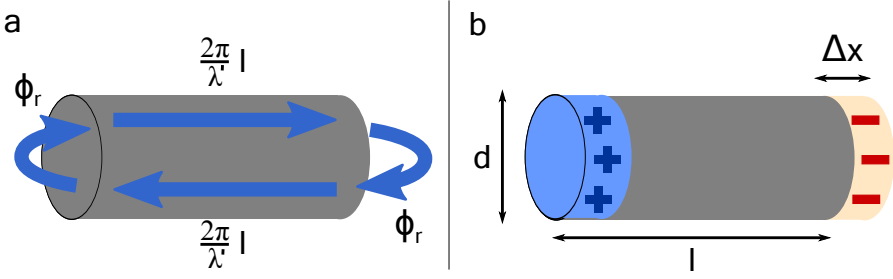
FIGURE 2.5. a) Fabry-Perot-model of a single nanowire. A wave traveling along the wire acquires a phase $\phi = \frac{2\pi}{\lambda} l$ and upon reflection at the caps an additional factor of ϕ_r. b) Mass-spring-model of a single nanowire, where the free electron gas is displaced by Δx inducing net charges at the ends.

CaF$_2$ have a small, positive and real ε_r in the same frequency range. Having found possible material pairs, the remaining question is how to excite surface-plasmon-polaritons. Figure 2.4 shows the dispersion relation for the parallel component of the wave vector of a plane wave in free space and for a SPP at a air-metal interface. Energy and momentum conservation dictates that excitation of the plasmon happens at the intersection of the two curves. Since no such crossing point exists (different momentum at every energy), it is not possible to directly excite SPPs with plane-wave illumination.

2.2.2 PARTICLE PLASMONS

In contrast to plane interfaces, it is possible to directly (by plane-wave illumination) excite surface plasmons on particles much smaller than the wavelength.[49] Imagine, for example, a small metal wire with a diameter of 10–100 nm, so that the penetration depth (skin depth) of the electric field is of the same order as the radius[a]. Combined with the strong curvature of the wire, this leads to a broad distribution of differently oriented wave vectors at the interface, of which some match the dispersion relation of the plasmon.

The excited surface plasmons are strongly localized on the wire and in the simplest case propagate as rotationally symmetric waves along the structure.[49,50] If we are dealing with a wire of finite length, like a rod, the ends act as discontinuities which can be described as mirrors at which the propagating wave is reflected with a phase jump Φ_r.[49] It is easy to imagine that we can find wavelengths λ' for a given length d of the metal rod where the phase difference δ between consecutive round trips is an integer n multiple of 2π, resulting in constructive interference:

$$\delta = 2\left(\frac{2\pi}{\lambda'} l + \Phi_r\right) = 2n\pi \quad n = 0, 1, 2, \ldots. \tag{2.30}$$

---

[a]Using Equation 2.11 we can estimate the skin depth (decay of the field magnitude to $1/e$) of gold ($\kappa \approx 38$) at 6 μm to be 13 nm.

Thus, a localized particle-plasmon-polariton (PPP) can be described as a standing electromagnetic wave on a metal nanorod.[51] This Fabry-Pérot model, besides providing an intuitive model for the plasmon resonance, also correctly captures the higher-order modes which have been observed in near-field probing experiments[51] (see also Fig 2.6). It is worth noting that the wavelength λ' of this PPP is smaller than the corresponding vacuum wavelength λ_0. Using the Drude model and assuming a subwavelength metal rod one can show that:

$$\lambda' = a + b\lambda_0, \tag{2.31}$$

where a and b are frequency independent parameters which are given by the geometry of the rod and end caps.[52]

It is instructive to introduce an alternative description where the localized surface plasmon is treated as the resonant displacement of the free electrons of the metal (mass-spring-model). We describe the nanorod as a cylinder with base $A = \pi(d/2)^2$ and length l (see Fig. 2.5). If the electron distribution of this rod is displaced by Δx relative to the lattice, net charges $\pm q$ accumulate at the ends. This charge accumulation is strongly dependent on the electron density n and leads to a Coulomb potential of the form:

$$V(\Delta x) = \frac{1}{4\pi\varepsilon_0}\frac{q^2}{d} = \frac{1}{4\pi\varepsilon_0}\frac{(neA)^2}{l}\Delta x^2, \tag{2.32}$$

where e is the electron charge. By expressing the spring constant as $D = \omega_{Res}^2 m$ where $m = m_e n A l$ represents the collective mass of all electrons, the restoring force can be written as:

$$F(\Delta x) = -\frac{\partial V}{\partial \Delta x} = -\frac{n^2 e^2}{2\pi\varepsilon_0}\frac{A^2}{l}\Delta x = -D\Delta x, \tag{2.33}$$

which allows us to determine the resonance frequency

$$\omega_{Res} = \frac{\omega_p}{2\sqrt{2}}\frac{d}{l}, \tag{2.34}$$

where $\omega_p = \sqrt{\frac{ne^2}{\varepsilon_0 m_e}}$ is the material specific plasma frequency. Although this model disregards higher-order resonances and does not accurately predict the precise spectral position of the plasmon resonance, it provides an intuitive picture for the resonance condition, and works very well for capturing general trends. Among others, it correctly predicts the scaling of the resonance frequency with the inverse of the aspect ratio $R = d/l$,[53] as well as the dependency of ω_{Res} on the charge carrier density (i.e. the metal used).[54]

2.3 NONLINEAR POLARIZATION

Most experiments in this thesis deal with the ultrafast dynamics of vibrational modes that are resonant in the mid-infrared, e.g. the amide I (6 μm) and the $NH_3{}^+$-bending
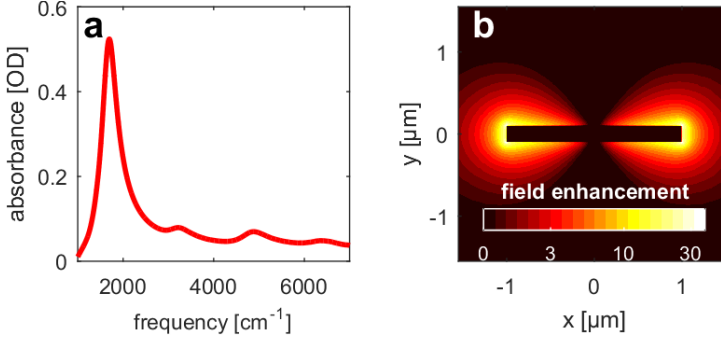
FIGURE 2.6. a) Linear infrared spectrum of gold nanorods on a CaF_2 substrate. In addition to the fundamental resonance at 1700 cm^{-1}, higher-order modes can be seen at ~3300 cm^{-1}, ~4900 cm^{-1}, ~6400 cm^{-1}. b) Finite-difference time-domain simulations of one gold nanorod (black bar in the center) on a CaF_2 substrate. The color scale shows the enhancement of the incident electric field at the resonance frequency of the nanoantenna.

vibration (7 μm). Unfortunately, there are no ultrafast, tunable laser systems which access this wavelength range directly. Instead, one usually starts with an intense light source in the visible or near-infrared (0.5–1.2 μm) and exploits the nonlinearity of the light-matter interaction to generate infrared wavelengths. Modern pulsed laser sources in the visible can generate electric field strengths of more than 10^9 V/m for which in many materials the linear relationship between the polarization and the electric field does not hold anymore. In this case we can express the induced polarization as a power series in the electric field $\vec{E}$[55]

$$P_i = \varepsilon_0 \left(\sum_{j=1}^{3} \chi_{ij}^{(1)} E_j + \sum_{j,k=1}^{3} \chi_{ijk}^{(2)} E_j E_k + \sum_{j,k,l=1}^{3} \chi_{ijkl}^{(3)} E_j E_k E_l + \dots \right), \quad (2.35)$$

where the tensors $\chi^{(n)}$ are the various expansion orders of χ with rank $n + 1$. By writing the products in Equation 2.35 we are assuming that all orders of χ are real, i.e. that the material reacts instantaneously to the applied electric field.[56] For light-conversion applications involving $\chi^{(2)}$ this is mostly valid since the involved crystals are transparent and can be assumed lossless in the frequency regions of interest. By expressing every expansion order n by a symbol $\vec{P}^{(n)}$ we can rewrite Equation 2.35 as a sum of linear $P^{(1)} = P^L$ and nonlinear terms P^{NL}:

$$\vec{P} = \vec{P}^{(1)} + \vec{P}^{(2)} + \vec{P}^{(3)} + \dots = \vec{P}^L + \vec{P}^{NL}. \quad (2.36)$$

The magnitude of the different susceptibility tensor elements strongly depends on the material and symmetry of the medium. For instance, the second order polarization vanishes inside the bulk of a centrosymmetric material. Therefore a non-vanishing second order polarization can only arise at the interface of a material or inside the bulk of a non-centrosymmetric material.[55,56]

For the following discussion we will drop the vectorial nature of the electric field and the polarization and consider $P^{(2)}$ for a noncentrosymmetric, nonlinear medium

in the presence of two monochromatic, linearly polarized plane waves propagating in the z-direction. We can write the total electric field as a superposition of the two scalar input fields, with $\omega_1 > \omega_2$:

$$E(t,z) = A_1 \cos(k_1 z - \omega_1 t) + A_2 \cos(k_2 z - \omega_2 t), \tag{2.37}$$

where A_n is the amplitude, k_n the wave vector and ω_n the frequency of the respective field. Inserting Equation 2.37 into the second order polarization $P^{(2)}$ yields:

$$P^{(2)} = \varepsilon_0 \chi^{(2)} E^2 = \varepsilon_0 \chi^{(2)} \left(0.5 A_1^2 \cos(2(k_1 z - \omega_1 t)) \right. \qquad \text{(SHG)} \tag{2.38}$$
$$+ 0.5 A_2^2 \cos(2(k_2 z - \omega_2 t)) \qquad \text{(SHG)} \tag{2.39}$$
$$+ A_1 A_2 \cos((k_1 + k_2)z - (\omega_1 + \omega_2)t) \qquad \text{(SFG)} \tag{2.40}$$
$$+ A_1 A_2 \cos((k_1 - k_2)z - (\omega_1 - \omega_2)t) \qquad \text{(DFG)} \tag{2.41}$$
$$\left. + 0.5(A_1^2 + A_2^2) \right). \qquad \text{(OR)} \tag{2.42}$$

This equation shows that the nonlinear polarization has new frequency components which were not present in the input fields. Specifically, the first two terms represent second harmonic generation (SHG) or the doubling of ω_1 and ω_2, the third term is the sum frequency (SFG) and the fourth term the difference frequency of the two input frequencies. The last term is constant in time and corresponds to a static polarization of the medium (optical rectification).

To simplify the discussion, we assume that the most dominant contribution originates from the DFG-term (Eq. (2.41)) where the ordering of the frequencies is given by: $\omega_1 > \omega_2 \geq \omega_3$. In general, all of the above frequency mixing processes are present, but by manipulating magnitude of the wave vectors of the input fields and the generated field, the conversion efficiency of specific processes can be selected, as will be shown below.

To investigate the light conversion process inside the nonlinear material, we insert the nonlinear polarization into the wave equation Eq. 2.4:

$$\frac{\partial^2 E(t,z)}{\partial z^2} - \frac{\varepsilon_r}{c^2} \frac{\partial^2 E(t,z)}{\partial t^2} = \mu_0 \frac{\partial^2 P^{NL}(t)}{\partial t^2}. \tag{2.43}$$

The nonlinear polarization acts as a source term which oscillates at ω_3:

$$P^{NL}(t,z) = P^{NL}(z) e^{-i\omega_3 t} + c.c., \tag{2.44}$$

which in turn drives an electric field with amplitude $\tilde{A}(z)$:

$$E(t,z) = \tilde{A}(z) e^{-i\omega_3 t} + c.c. \tag{2.45}$$

at the same frequency. We assume that the field amplitudes $\tilde{A}$, A_1 and A_2 are time-independent. By executing the time derivative we can remove the time-dependence from Eq. (2.43):

$$\frac{\partial^2 \tilde{A}(z)}{\partial z^2} + \frac{\varepsilon_r \omega_3^2}{c^2} \tilde{A}(z) = -\mu_0 \omega_3^2 P^{NL}(z). \tag{2.46}$$

The amplitude of the generated electric field is explicitly dependent on the position, since it will increase or decrease as the input fields propagate through the material. We make the assumption that the higher-order terms of the expansion in Eq. 2.36 only contribute a small correction to the linear term. Therefore, it is expected that the amplitude will vary slowly over multiple optical cycles. This is called the slowly varying envelope approximation[55, 56] and it allows us to separate the amplitude $\tilde{A}(z) = A(z)e^{ikz}$ of the generated field into a rapidly varying component e^{ikz} and a slowly evolving envelope $\tilde{A}(z)$. With this we can simplify the first term in Eq. (2.43):

$$\frac{\partial^2 A(z)e^{ikz}}{\partial z^2} = \left(-k^2 A(z) + 2ik\frac{\partial A(z)}{\partial z} + \frac{\partial^2 A(z)}{\partial z^2}\right)e^{ikz} \tag{2.47}$$

$$\approx \left(-k^2 A(z) + 2ik\frac{\partial A(z)}{\partial z}\right)e^{ikz} \tag{2.48}$$

by assuming $\left|ik\frac{\partial A(z)}{\partial z}\right| \gg \left|\frac{\partial^2 A(z)}{\partial z^2}\right|$. Combining Eq. (2.44) and Eq. (2.48) we can rewrite the wave equation Eq. (2.43) in its general form:

$$2ik\frac{\partial A}{\partial z}e^{ikz} = \mu_0\omega^2 P^{NL}. \tag{2.49}$$

By replacing the nonlinear polarization with the DFG-term from Eq. (2.42), we arrive at:

$$2ik\frac{\partial A_3}{\partial z}e^{ik_3 z} = -\frac{2\omega_3^2}{c^2}\chi^{(2)}A_1 A_2 e^{i(k_1 - k_2)z}. \tag{2.50}$$

The right-hand side of the equation can be interpreted as the spatially modulated polarization, with wavelength $2\pi/(k_1 - k_2)$, driving an electric field; and the left hand side is the generated electric field with wavelength $2\pi/k_3$. The efficiency of the nonlinear light conversion is dictated by the wave vector mismatch $\Delta k = k_1 - k_2 - k_3$ between the polarization and the wave front of the generated field. This means, that as long as Δk is non-vanishing, there exists a point $l_c = \pi/\Delta k$ at which the generated field has a phase shift of π relative to the field generated at $z = 0$. This destructive interference results in an energy flow from E_3 back to E_1 and E_2. The coherence length l_c defines the maximum path length up to which the amplitude of the generated field increases.

Under most conditions, even when employing materials with strong optical nonlinearity, the build up of E_3 will be negligible, since $\Delta k \neq 0$. To understand why $\Delta k \neq 0$ we can rewrite the wave vector mismatch:

$$\Delta k = \frac{n_1\omega_1}{c} - \frac{n_2\omega_2}{c} - \frac{n_3\omega_3}{c} \tag{2.51}$$

$$\Delta k = \frac{1}{c}\left(\omega_2(n_1 - n_2) + \omega_3(n_1 - n_2)\right). \tag{2.52}$$

In the absence of a resonance, most materials exhibit normal dispersion ($n(\omega_1) > n(\omega_2)$ for all $\omega_1 > \omega_2$), in which case the wave vector mismatch in the last equation is always greater than zero. It is, nevertheless, possible to achieve $\Delta k = 0$ by using

a technique called phase-matching, which employs a class of materials which are nonlinear and birefringent. In these materials, the refractive index strongly depends on the polarization and propagation direction of the electric field. Therefore, perfect phase-matching can be achieved by adjusting the beam polarization and choosing the correct crystal orientation.[55,56] In our setup, we use this approach to effectively convert 800 nm light to the mid-infrared (Section 3.1).

2.4 NONLINEAR INFRARED SPECTROSCOPY

Most of the experiments presented in this thesis involve nonlinear infrared spectroscopy. In this section we will introduce the theoretical foundation for infrared light-absorption, discuss the basic principles of pump-probe spectroscopy and show how it can be used to explore ultrafast molecular dynamics.

2.4.1 INFRARED ABSORPTION

Molecular vibrations can be described as quantum mechanical harmonic oscillators.[57–59] The time-independent Hamiltonian of an oscillator with mass m and spring constant k is given by:

$$\hat{H}_0 = \frac{\hat{p}^2}{2m} + \frac{1}{2}k\hat{x}^2, \tag{2.53}$$

where $\hat{p}$ and $\hat{x}$ refer to the momentum and position operator, respectively. The energies E_ν for the allowed states $|\Psi\rangle$ of the system can be found by solving the time-independent Schrödinger equation:[60,61]

$$\hat{H}_0 |\Psi\rangle = \hat{E} |\Psi\rangle. \tag{2.54}$$

By determining the eigenvalues of the equation one can find the state energies:

$$E_\nu = \hbar\omega_0(\nu + \frac{1}{2}), \tag{2.55}$$

where ν is the vibrational quantum number and $\omega_0 = \sqrt{k/m}$ the fundamental frequency of the oscillator. The system described so far is stationary, and it will not undergo state transitions because the Hamiltonian is independent of time. A time-dependent perturbation $V(t)$ of the static Hamiltonian:

$$\hat{H}(t) = \hat{H}_0 + \hat{V}(t) \tag{2.56}$$

is necessary to induce a state transition. In spectroscopy, the perturbation is given by an oscillating electric field which acts on the dipole moment (operator) $\vec{\hat{\mu}}$ of the molecule:[57]

$$\hat{V}(t) = -\frac{1}{2}\vec{\hat{\mu}} \cdot \vec{E}(t) = -\frac{1}{2}\vec{\hat{\mu}}\vec{E}_0\left(e^{-i\omega t} + e^{i\omega t}\right). \tag{2.57}$$

Here we have used the electric dipole approximation which assumes that the spatial extent of the electromagnetic wave is much larger than the size of the oscillator:

$e^{i\vec{k}\vec{x}-i\omega t} \approx e^{-i\omega t}$. The temporal evolution of the wave function $|\Psi\rangle$ is described by the time-dependent Schrödinger equation:[60,61]

$$i\hbar \frac{\partial}{\partial t}|\Psi\rangle = \hat{H}(t)|\Psi\rangle. \tag{2.58}$$

For a small perturbation, the transition rate R_{es} per unit time from an initial state $|s\rangle$ with energy E_s to a final state $|e\rangle$ with energy E_e is in first order given by Fermi's golden rule:[60,61]s

$$R_{es} = \frac{2\pi}{\hbar^2}|\langle e|\hat{V}(t)|s\rangle|^2(\delta(\omega_{es}-\omega)+\delta(\omega_{es}+\omega)), \tag{2.59}$$

where $\omega_{es} = (E_s - E_e)/\hbar$. Substituting the perturbation from the light field and writing the inner product $\vec{\hat{\mu}}\cdot\vec{E}$ in terms of the angle θ between $\vec{E}$ and $\vec{\hat{\mu}}$, we can reformulate the transition rate to:

$$R_{es} = \frac{\pi}{2\hbar^2}|E_0|^2\cos^2(\theta)\big(\delta(\omega_{es}-\omega)+\delta(\omega_{es}+\omega)\big)|\langle e|\hat{\mu}|s\rangle|^2. \tag{2.60}$$

Equation 2.60 provides much information about light absorption. The $\cos^2(\theta)$ factor implies that the relative orientation of the transition dipole moment and the electric field dictates the absorption. The two Dirac-δ functions ensure energy conservation: the amount of energy extracted ($\delta(\omega_{es}-\omega)$) from or provided ($\delta(\omega_{es}+\omega)$) to the electric field has to be exactly the energy difference between two states.

To evaluate the last factor in Eq. 2.60, it is convenient to expand $\vec{\hat{\mu}}(x)$ in a Taylor series around the equilibrium $x = x_0$:

$$\langle e|\vec{\hat{\mu}}(x)|s\rangle\Big|_{x\approx x_0} = \underbrace{\vec{\mu}(x_0)\langle e|s\rangle - \frac{\partial\vec{\mu}(x_0)}{\partial x}x_0\langle e|s\rangle}_{0\,for\,e\neq s} + \frac{\partial\vec{\mu}(x_0)}{\partial x}\langle e|\hat{x}|s\rangle\dots \quad . \tag{2.61}$$

The first two terms are zero for state transitions, due to the orthogonality of the vibrational states. By using only the first order of the Taylor expansion, the selection rules are limited to $e = s \pm 1$. To also capture multi-quantum absorption, like overtones and combination bands, higher-order terms of the potential (anharmonicity) or the expansion of $\vec{\hat{\mu}}$ need to be included. Although it is possible to excite such higher-order transitions, their cross section usually rapidly decreases with the number of vibrational quanta involved[b]!

Lastly, the $\frac{\partial}{\partial x}\vec{\mu}$ term implies that for a mode to be excitable by the electric field, the transition dipole moment of the molecule has to change as a result of the vibrational motion. This explains why the symmetric stretch vibration of H_2O has an infrared absorption but the same vibration in CO_2 does not.
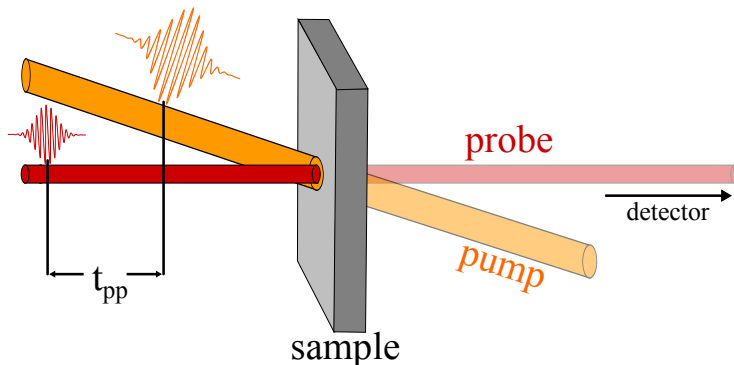
FIGURE 2.7. Pump-probe experiment. An intense pump pulse excites a significant amount of molecules in its focal spot (in the sample). The excited molecules are monitored by a weak probe pulse which interrogates the sample at a time delay t_{pp} after the pump pulse.

2.4.2 ANHARMONIC OSCILLATOR

It is easy to see that the harmonic potential used in the previous section is not a realistic representation of a vibration. The repulsive force should become infinitely large as the distance between two atoms (or chemical groups) vanishes due to electrostatic repulsion; for $x \to \infty$, the restoring force should become zero upon dissociation. For a more realistic representation, one can expand the vibrational potential to include higher-order terms:

$$\hat{H} = \underbrace{\frac{1}{2m}\hat{p}^2 + \frac{1}{2}k\hat{x}^2}_{H_0} + \underbrace{c\hat{x}^3 + d\hat{x}^4}_{\hat{H}'}, \qquad (2.62)$$

where c and d are expansion coefficients. In the last equation we have also rewritten the harmonic Hamiltonian $\hat{H}_0$ as a function of the ladder operators:[60,61]

$$\hat{x} = \sqrt{\frac{\hbar}{2m\omega}}(\hat{a}^\dagger + \hat{a}) \qquad\qquad \hat{p} = i\sqrt{\frac{\hbar m\omega}{2}}(\hat{a}^\dagger - \hat{a}). \qquad (2.63)$$

These operators simplify the calculation of the energy eigenvalues, since they essentially increase or decrease the energy of the oscillator by one quantum when they operate on the energy eigenstate $|n\rangle$:

$$\hat{a}^\dagger |n\rangle = \sqrt{n-1}\,|n+1\rangle \qquad (2.64)$$
$$\hat{a}\,|n\rangle = \quad\sqrt{n}\,|n-1\rangle. \qquad (2.65)$$

It is straightforward to show that the expectation value of the cubic term ($\langle n|\hat{x}^3|n\rangle$) always equates to zero since all terms in the expansion of x^3 have an uneven number

---

[b]Some of these transitions can still be observed. For example, for long optical path lengths H_2O has a blueish color relative to D_2O which originates from a four-quantum transition (~760 nm).

of creation $\hat{a}$ and annihilation $\hat{a}^{\dagger}$ operators and therefore are not quantum conserving. Using perturbation theory to first order, the energy levels corresponding to $\hat{H}$ can be written as[57,60]

$$E_n = E_n^{(0)} + d \left\langle n^{(0)} \left| \hat{x}^4 \right| n^{(0)} \right\rangle \tag{2.66}$$

$$= \hbar\omega \left(n + \frac{1}{2} \right) + \frac{3d\,\hbar^2}{2m^2\omega^2} \left(n^2 + n + \frac{1}{2} \right), \tag{2.67}$$

where $n^{(0)}$ and $E_n^{(0)}$ are the states and the corresponding eigenenergies of the harmonic oscillator (zeroth order). Since the restoring force becomes weaker with increasing displacement, d has to be negative, resulting in lower energy eigenvalues than for the harmonic oscillator. Furthermore, the quartic term in the Hamiltonian leads to **non**equally spaced energy levels. This has very important consequences for pump-probe spectroscopy, where we simultaneously investigate the $|0\rangle \rightarrow |1\rangle$-transition and the $|1\rangle \rightarrow |2\rangle$-transition. For the harmonic case, both transitions have the same frequency.

For the following sections it is important to understand which energy states are usually accessible under normal lab conditions (room temperature). The probability for a mode to be thermally excited at a temperature T from state $|s\rangle$ to $|e\rangle$ is given by Boltzmann statistics:

$$\propto e^{-\frac{E_e - E_s}{k_B T}}, \tag{2.68}$$

where k_B is the Boltzmann constant. As an example, let us consider the NH_3^+ bending vibration which will be studied in Chapters 7 and 8 ($\omega \approx 1470$ cm^{-1}). From this frequency we can estimate that the excited state population of this vibration is only 0.1% at room temperature. Since all modes considered in this thesis are of similar or even higher frequency (>1470cm^{-1}), we will assume that their population manly occupies the ground state.

2.4.3 PUMP-PROBE SPECTROSCOPY

Linear infrared spectroscopy provies structural information about the interrogated molecules. For example, it provides information on the functional chemical groups present inside the molecules, on the strength of their hydrogen bonds, and, in the case of proteins, on their secondary structure. By extending the experiments to the nonlinear regime, we can gain additional information about dynamic processes, such as vibrational relaxation and molecular reorientation, and about the coupling between different vibrational modes.

In infrared pump-probe spectroscopy, an intense pump pulse is used to saturate a vibration and to prepare a nonequilibrium state. A subsequent weak probe pulse is used to interrogate the excited system. In the following chapters we are going to look at the amide I' and the symmetric NH_3-bend vibrations, which have a decay rate of ~1 ps. The ultrafast processes involving these mode can be observed by introducing a very well-defined time delay t_{pp} between the pump and probe pulses, which can be scanned with high precision over multiple orders of magnitude (fs–ns).
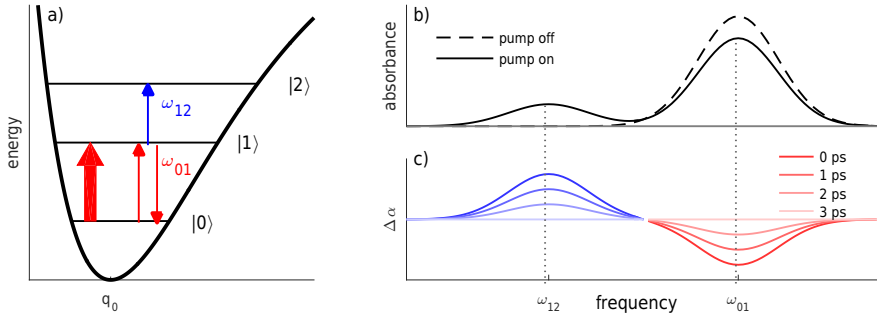
FIGURE 2.8. a) First three levels of an anharmonic vibrational potential. The pump (bold red arrow) excites part of the ground-state $|0\rangle$ population to the first excited state $|1\rangle$. Shortly thereafter the probe pulse exhibits a decreased absorption at the fundamental frequency ω_{01} due to the pump-induced ground-state depletion and stimulated emission from $|1\rangle$. In addition, the probe is absorbed more at ω_{12} because $|1\rangle$ oscillators can be excited to $|2\rangle$. b) shows the linear spectrum measured with and without the preceding pump interaction. c) Pump-probe delay dependent absorption change $\Delta\alpha$.

In practice, an absorption change is measured by comparing the absorption of the probe by the sample in the presence and absence of a pump excitation:

$$\Delta\alpha^{probe} = \alpha^{probe}_{pump_{on}} - \alpha^{probe}_{pump_{off}}. \tag{2.69}$$

For clarity, we will omit the superscript in the following. The second term is just the linear absorption of the probe:

$$\alpha(\omega) = n\sigma_{01}(\omega), \tag{2.70}$$

where n is the concentration of molecules per unit area and σ_{01} the spectrum of the ground state absorption ($|0\rangle \rightarrow |1\rangle$). The interaction with the pump leads to three effects:

1. **ground-state depletion:** The probe light is absorbed less at the fundamental transition $\sigma_{01}(\omega)$ since a fraction of the oscillators N are excited to the first excited state $|1\rangle$.

2. **stimulated emission:** The fraction of excited molecules N can be stimulated to the ground state by emitting a photon. This can also be interpreted as a decrease in absorption at the transition σ_{01}, since more photons are leaving the sample than have entered.

3. **excited-state absorption:** The fraction of excited molecules N can be excited further to the second excited state leading to absorption at slightly lower frequencies ω_{12} due to the anharmonicity of the vibrational potential.

Over time the excited molecules will relax from the excited state to the ground state:
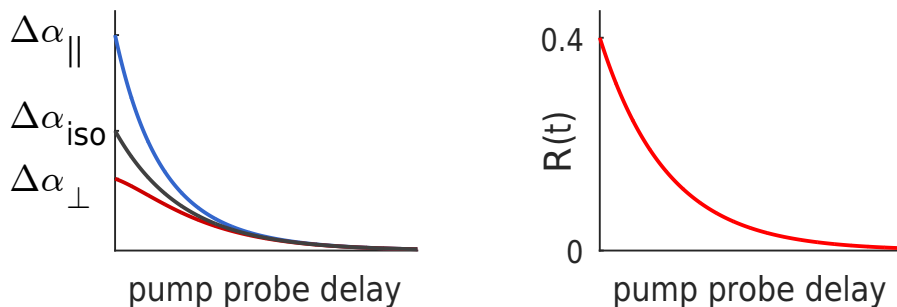
$$N(t) = N(0)e^{-\frac{t}{\tau}}, \tag{2.71}$$

FIGURE 2.9. Polarization-dependent absorption change. By measuring the absorption change in parallel $\Delta\alpha_\parallel$ and perpendicular $\Delta\alpha_\perp$ polarization, relative to the pump polarization, the isotropic $\Delta\alpha_{iso}$ and anisotropic $R(t)$ signal can be constructed.

where we have assumed a direct decay to the ground state with relaxation time τ. Hence, we can write for the pump induced absorption change:

$$\Delta\alpha(\omega,t) = (n - N(t))\sigma_{01}(\omega) - N(t)\sigma_{01}(\omega) + N(t)\sigma_{12}(\omega) - n\sigma_{01}(\omega) \quad (2.72)$$

$$= \Big(\underbrace{\sigma_{12}(\omega)}_{ESA} - \underbrace{2\sigma_{01}(\omega)}_{bleach} \Big) N(0) e^{-\frac{t}{\tau}}. \quad (2.73)$$

One usually refers to the negative terms of the absorption change as bleach and to the positive term as excited state absorption (ESA). Figure 2.8 summarizes this section in a schematic way.

2.4.4 POLARIZATION DEPENDENCE

One of the key pieces of information that we can access with pump-probe spectroscopy is the vibrational relaxation rate. Ideally, one would just need to monitor the amplitude of the pump-probe signal as a function of delay time to determine the excited-state population and, thereby, the vibrational lifetime. However, a complication arises because (in addition to the excited state population) there are other factors that can affect the amplitude of the pump-probe signal, for example reorientation (rotation) of the excited molecule. In a polarization-resolved pump-probe experiment, where all pulses are linearly polarized, we can construct the isotropic signal:

$$\Delta\alpha(t)_{iso} = \frac{\Delta\alpha(t)_\parallel + 2\Delta\alpha(t)_\perp}{3}, \quad (2.74)$$

which only depends on the number of excited molecules.[62] Here, $\Delta\alpha_\parallel$ and $\Delta\alpha_\perp$ are the absorption changes measured with a probe polarization parallel and orthogonal to the pump polarization, respectively.[c] It is important to realize that, due to the

---

[c]The factor of 2 enters due to the azimuthal symmetry of the excited dipole. If the pump beam linearly polarized (e.g. E_z), there are two different probing polarizations which result in the same absorption change (i.e. E_x and E_y).

$\cos^2\theta$ excitation dependency, the absorption change directly after excitation is highly anisotropic ($\Delta\alpha_\parallel > \Delta\alpha_\perp$). By keeping track of the degree of anisotropy, we gain access to the average transition dipole orientation of the excited molecules, relative to the pump polarization as a function of delay time. This information can, for example, be used to determine the reorientation time of small molecules like water[d]. The time-dependent anisotropy can be constructed as:[62]

$$R(t) = \frac{\Delta\alpha_\parallel(t) - \Delta\alpha_\perp(t)}{\Delta\alpha_\parallel(t) + 2\Delta\alpha_\perp(t)}. \tag{2.75}$$

This definition removes the contribution of the vibrational relaxation to the anisotropy by normalizing to the isotropic signal. The experimental anisotropy provides a measure for the orientation correlation function of the transition dipole moment. More precisely, the anisotropy is related to the angular displacement of the transition dipole moment during the pump-probe delay via:

$$R(t) = \frac{2}{5}\left\langle P_2(\vec{\mu}(0)\cdot\vec{\mu}(t))\right\rangle \tag{2.76}$$

$$= \frac{2}{5}\left\langle \frac{1}{2}\left(3\cos^2\theta - 1\right)\right\rangle, \tag{2.77}$$

where $\langle...\rangle$ is the ensemble average and $P(x)_2 = (3x^2 - 1)/2$ is the second order Legendre polynomial. It is insightful to look at the limiting cases of Equation 2.77 for an isotropic sample.

If $\mu(0)$ and $\mu(t)$ are parallel $R(t)$ is $\frac{2}{5}$. That is, the detected molecules have exactly the same orientation as the exited ones which is, for example, the case directly after excitation ($t_{pp} \sim 0$ ps) since there was not enough time yet for the molecules to undergo any kind of motion. Shortly after excitation, the molecules will undergo (rotational) diffusion and possibly transfer energy to other oscillators. Thus, for long pump-probe delays the molecular ensemble will approach an isotropic distribution with $\langle\cos^2\theta\rangle = 1/3$ and the anisotropy will decay to $R(t) = 0$. If $\mu(0)$ and $\mu(t)$ are perpendicular, $R(t)$ is $-\frac{1}{5}$.

In a polarization-resolved experiment we usually measure the decay of the anisotropy. The decay mechanism strongly depends on the system. In water, for example, both the reorientation of the individual molecules ($\sim$1–5 ps[63,64]) but also resonant energy transfer ($<$200 fs[65,66]) contribute to the decay of the anisotropy. In big molecules like proteins the anisotropy tends to stay close to 0.4 within the probed time interval since the rotational diffusion is slow compared to the vibrational lifetime.

2.5   TWO-DIMENSIONAL INFRARED SPECTROSCOPY

Two-dimensional infrared spectroscopy (2DIR) provides several advantages over conventional pump-probe spectroscopy. 2DIR can be seen as a pump-probe

---

[d]For example, the reorientation time of OD vibration of HOD in H_2O is 2.5 ps.[63]
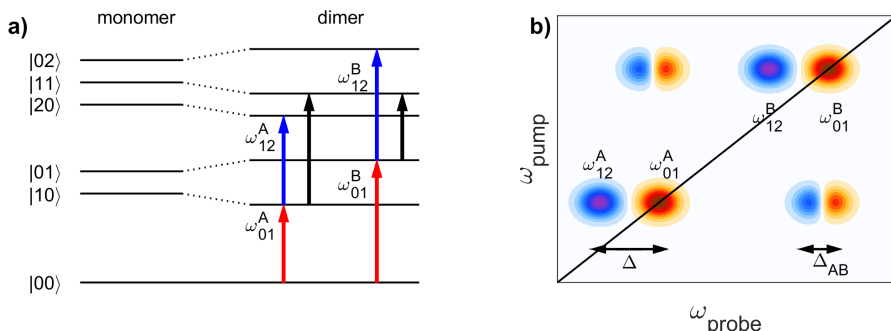
FIGURE 2.10. Coupling in 2DIR. a) level diagram of two vibrational modes in the monomer and weakly coupled configuration. $|ij\rangle$ represent states with i quanta in mode A and j quanta in mode B, and the associated line represents the energy level. Red arrows indicate ω_{01} transitions (bleach), blue arrows the ω_{12} transitions (ESA) and black arrows cross excitation. b) corresponding 2DIR map.

experiment resolved both along the probe and the pump frequency. The additional resolution along the pump axis gives more detailed access to the time evolution of spectral lineshapes (spectral diffusion), and it allows us to identify and characterize anharmonic coupling between vibrations.

Figure 2.10 shows the energy levels for two coupled vibrations and the corresponding 2DIR spectrum. The spectrum can roughly be divided into two parts: peak pairs along the diagonal consisting of a negative bleach ($|0\rangle \rightarrow |1\rangle$) and a positive excited state ($|1\rangle \rightarrow |2\rangle$) absorption of the individual vibrational modes; peak-pairs on the off-diagonal (cross-peaks) which also consist of a positive and a negative part. The appearance of cross-peaks means that excitation of vibration A induces a transient signal from vibration B. Therefore, the mere presence of cross-peaks is a very valuable piece of information since it directly implies coupling between two vibrational modes. By investigating the dynamics of the cross-peaks we can discriminate between different coupling mechanisms, such as anharmonic interaction or energy transfer. In addition, by analyzing the cross-peak anharmonicity (bleach-induced absorption splitting) we can get an indication about the coupling strength, and by looking at the cross-peak anisotropy one can extract the angle between the coupled transition dipoles.

The lineshape of every resonance provides insight into the local environment of the respective vibrational mode. In contrast to linear infrared spectroscopy, in 2DIR it is possible to directly disentangle contributions from homogeneous and inhomogeneous line broadening by inspecting the lineshapes at early t_{pp}-delays. By following the spectral evolution of a peak, one gains access to the timescale of the local fluctuations, which for molecules in solutions often can be related to the solvation dynamics.

2.5.1 ANHARMONIC INTERACTION

Next, we are going to inspect the coupling between two vibrational modes where, for simplicity, we will focus on a weakly coupled dimer and provide a flavor for the general information content accessible by 2DIR. The coupling between two vibrations, which we describe in their respective local mode coordinates, $\hat{q}_A$ and $\hat{q}_B$, is determined by the potential energy surface. Expanding the potential around the local mode coordinates q_i and keeping only the bilinear term yields the following expression for the coupling term:[67]

$$\hat{V}(\hat{q}_A, \hat{q}_B) \approx 2\beta_{AB}\hat{q}_A\hat{q}_B, \tag{2.78}$$

where β_{AB} is the coupling constant. Rewriting the potential in terms of ladder operators $\hat{q}_i = 1/\sqrt{2}(\hat{b}_i^\dagger + \hat{b}_i)$ and keeping only the quantum conserving terms leads to

$$\hat{V}_{AB} = \beta_{AB}(\hat{b}_A^\dagger\hat{b}_B + \hat{b}_B^\dagger\hat{b}_A). \tag{2.79}$$

We will describe the energy of the second excited state by:

$$E_{A,B}^{(2)} = 2E_{A,B}^{(1)} - \Delta_{A,B}, \tag{2.80}$$

where $\Delta_{A,B}$ is the correction term used to account for anharmonicity of the potential. For simplicity, we are going to assume equal diagonal anharmonicies $\Delta = \Delta_A = \Delta_B$ for both vibrational modes. With this, we can write the Hamiltonian for two weakly coupled anharmonic oscillators:[67]

$$\hat{H} = \hbar\omega_A\hat{b}_A^\dagger\hat{b}_A + \hbar\omega_B\hat{b}_B^\dagger\hat{b}_B - \frac{\Delta}{2}\hat{b}_A^\dagger\hat{b}_A^\dagger\hat{b}_A\hat{b}_A - \frac{\Delta}{2}\hat{b}_B^\dagger\hat{b}_B^\dagger\hat{b}_B\hat{b}_B, \\ +\beta_{AB}(\hat{b}_A^\dagger\hat{b}_B + \hat{b}_B^\dagger\hat{b}_A) \tag{2.81}$$

where we have ignored the zero-point energies. The first two terms represent the harmonic-oscillator Hamiltonian for two independent oscillators A and B. The third and fourth terms are phenomenological correction terms needed to account for the anharmonic character of both oscillators. Finally the last term represents the coupling between the two oscillators. Since 2DIR (third-order) spectroscopy can only access states up to two quantum excitations, we work with a reduced basis set $\{|ij\rangle\} = \{|00\rangle, |01\rangle, |10\rangle, |02\rangle, |20\rangle, |11\rangle\}$, where i and j represent the number of excitation on site A and B, respectively. The Hamiltonian matrix in this basis is given by:[67,68]

$$\hat{H} = \begin{pmatrix} 0 & & & & & \\ & \hbar\omega_A & \beta_{AB} & & & \\ & \beta_{AB} & \hbar\omega_B & & & \\ & & & 2\hbar\omega_A - \Delta & 0 & \sqrt{2}\beta_{AB} \\ & & & 0 & 2\hbar\omega_B - \Delta & \sqrt{2}\beta_{AB} \\ & & & \sqrt{2}\beta_{AB} & \sqrt{2}\beta_{AB} & \hbar\omega_A + \hbar\omega_B \end{pmatrix}. \tag{2.82}$$

The Hamiltonian consists of three blocks corresponding to zero, one, and two quanta of excitation. The energies of the coupled states can be found by diagonalizing this Hamiltonian. Since the matrix is block diagonal, the sub-matrices can be diagonalized independently. For the one-quantum case the energies are given by:

$$E_{A,B}^{(1)} = 0.5 \left(\hbar\omega_A + \hbar\omega_B \mp \sqrt{4\beta_{AB} + (\hbar\omega_B - \hbar\omega_A)^2} \right). \tag{2.83}$$

In the limit of weak coupling, $|\beta_{AB}| \ll |\hbar\omega_A - \hbar\omega_B|$, the excitation is mainly localized on one of the modes. The corresponding energies are given by the monomer energies slightly shifted by the coupling term:

$$E_{A,B}^{(1)} \approx \hbar\omega_{A,B} \mp \frac{2\beta_{AB}^2}{\hbar\omega_B - \hbar\omega_A}. \tag{2.84}$$

In the other extreme, when both oscillators are strongly coupled $|\beta_{AB}| \gg |\hbar\omega_A - \hbar\omega_B|$, the excitation is delocalized over both modes. In this case, the energies are given by the mean value of the energies of the uncoupled oscillators shifted by the coupling interaction:

$$E_{A,B}^{(1)} \approx 0.5(\hbar\omega_A + \hbar\omega_B) \mp \beta_{AB}. \tag{2.85}$$

Lastly, the energy for the simultaneous excitation of both sites is given by:

$$E_{AB}^{(2)} = E_A^{(1)} + E_B^{(1)} - \Delta_{AB}, \tag{2.86}$$

where Δ_{AB} is the off-diagonal anharmonicity. The last equation can be interpreted as a shift of the spectrum of one vibration, upon excitation of the other. Finding an analytical expression for Δ_{AB} is only possible for the degenerate case $\omega_A = \omega_B$.[67] However, by assuming weak coupling, one can use second order perturbation theory and show that the energy correction:[69]

$$\Delta_{AB} = \frac{4\Delta\beta_{AB}^2}{(\hbar\omega_A - \hbar\omega_B)^2} \tag{2.87}$$

is directly dependent on the coupling term β_{AB}, the energy gap between the two modes, and the diagonal anharmonicity. The seperation between the bleach and the induced absorption of a cross-peak are dictated by the off-diagonal anharmonicity. Hence, it is possible to extract Δ_{AB} and thereby the coupling term β_{AB} from the 2DIR spectrum.

In this context, it is interesting to note that diagonal anharmonicity is essential to observe any peak (doublets) in 2DIR, since without it the bleach and excited state absorption of every peak (diagonal and cross) would perfectly overlap and cancel each other out exactly. Finally, it should be noted that the coupling strength β_{AB} is not directly accessible in linear spectroscopy but it can be extracted from a 2DIR spectrum at one pump-probe delay.[25, 68, 70]
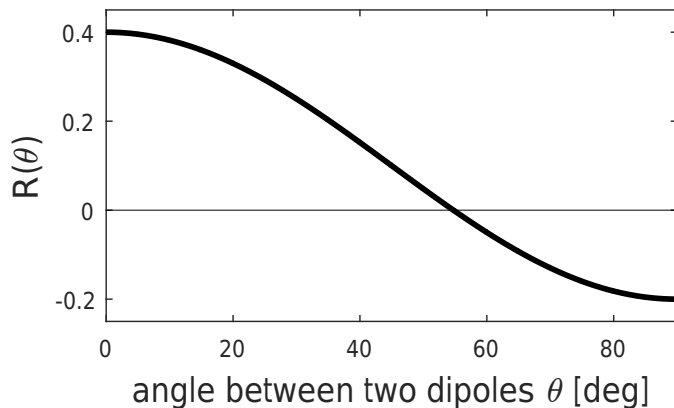
FIGURE 2.11.   Cross-peak anisotropy as function of the angle-between the two involved vibrations.

2.5.2   ANISOTROPY OF CROSS-PEAKS

In Section 2.4.4 we saw that anisotropy measurements provide information abouth the orientational motion of (the transition dipole moment of) a molecular vibration. In a very similar manner, the anisotropy of a cross-peak can be used to deduce the relative orientation of two different molecular vibrations (i.e. the angle between their transition dipole moments).

Let us assume that we are inspecting two spectrally separated but still coupled vibrations. In a narrow band excitation experiment where the pump only overlaps with one of the vibrational modes the angle dependence of the anisotropy is the same as for the diagonal peaks:

$$R(\theta) = \frac{2}{5} \langle P_2(\theta) \rangle \quad \text{with} \quad P_2(\theta) = \frac{1}{2} \left(3 \cos^2(\theta) - 1 \right), \tag{2.88}$$

where θ denotes the angle between the transition dipoles. Therefore, by measuring the anisotropy of the cross-peak and using Eq. (2.88) we can directly extract the relative orientation of the two vibrational modes. In addition, the time-dependence of the cross-peak ansisotropy can provide information about the persistence time of a given configuration. For an extended description of polarization dependence of cross peaks in different experimental geometries and their delay time dependence the reader is referred to Ref.[71] and.[67]

2.5.3   ENERGY TRANSFER

The previous section discussed how cross-peaks can arise from an anharmonic interaction. In this section it will be shown that energy or population transfer can also lead to cross-peaks. Cross-peaks which originate from energy or population transfer can be identified by a delayed ingrowth of their amplitudes since the exchange happens on a timescale longer than the pulse duration ($\sim$100 fs). For most systems

the energy transfer is mediated by a constantly changing local environment. This pulling and pushing of the molecules results in fluctuations of the local side energies $E_i(t) = \bar{E}_i + \delta E_i$ and of the coupling terms $\beta(t) = \bar{\beta} + \delta\beta(t)$. Here $\delta E_i(t)$ and $\delta\beta(t)$ stand for the fluctuating parts of $E_i(t)$ and $\beta(t)$. We gain insight into the effect of these fluctuations by extending the previously introduced one-quantum Hamiltonian (Eq. (2.82)) for a coupled dimer:[72]

$$H(t) = \begin{pmatrix} \bar{E}_A + \delta E_A(t) & \bar{\beta}_{AB} + \delta\beta(t) \\ \bar{\beta}_{AB} + \delta\beta(t) & \bar{E}_B + \delta E_B(t) \end{pmatrix}. \tag{2.89}$$

Using the perturbative expansion to zeroth order, and assuming the weak coupling limit ($\beta \ll \Delta E = |\bar{E}_B - \bar{E}_A|$), one can diagonalize the Hamiltonian with respect to its time average and use Fermi's golden rule ($P_{ij} = k_{ij}T$) to express the cross-relaxation rate as:[72]

$$\begin{aligned} k_{ij} = \frac{1}{\hbar^2} \int_{-\infty}^{+\infty} & \Big(\langle \delta\beta(0)\delta\beta(t) \rangle \\ & + \frac{2\beta}{\Delta E} \langle \delta\beta(0)\delta\Delta E(t) \rangle + \Big(\frac{\beta}{\Delta E}\Big)^2 \langle \delta\Delta E(0)\delta\Delta E(t) \rangle \Big) e^{\frac{i}{\hbar}\Delta E t} \, dt \end{aligned} \tag{2.90}$$

Here $\langle ... \rangle$ denotes the ensemble average, and $\delta\Delta E = \delta E_B(t) - \delta E_A(t)$. Since we assumed weak coupling, we discard the last two terms ($\frac{\beta}{\Delta E} \ll 1$). If the coupling fluctuations are Gaussian and Markovian[e], Kubo showed that the ensemble average can be written as[73]

$$\langle \delta\beta(0)\delta\beta(t) \rangle = d^2 e^{-\frac{t}{\tau}}, \tag{2.91}$$

where d is the amplitude of the fluctuation and τ the correlation time. Combining Eq. (2.90) and Eq. (2.91) we can find an expression for the transfer rate:

$$k = \frac{2d^2\tau}{\hbar^{-2} + \Delta E^2 \tau^2}. \tag{2.92}$$

The last equation shows that the transfer rate is about inversely proportional to the correlation time and directly proportional to the square of the fluctuation amplitude d. Since local fluctuations often originate from the dynamics of the solvent, the choice of the solvent can be used to enhance or decrease the transfer rate between two modes. Lastly, we remark that it may seem that there is an inconsistency in this treatment as energy does not appear to be conserved, i.e., there is an energy mismatch between the initial and the final state. This apparent inconsistency is, however, resolved if one realizes that the energy mismatch is taken up by the low-frequency solvent modes that are responsible for the fluctuations $\delta\beta(t)$.[69,74]

2.5.4 SPECTRAL DIFFUSION

In the previous section we have shown how fluctuations of the coupling term ($\delta\beta$) can induce energy transfer between two modes. In this section we will

---

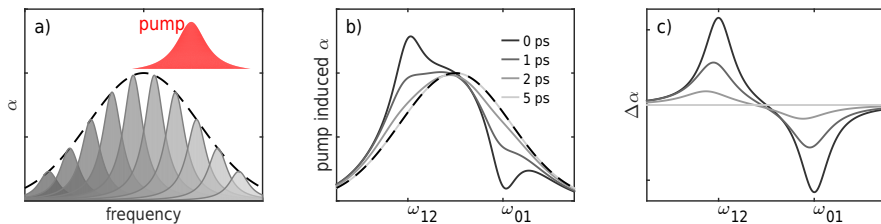[e]The future state only depends on the present state of the system and not on the past.

FIGURE 2.12. Hole burning experiment. a) Illustration of an inhomogeneously broadened vibrational mode. By using a narrowband pump pulse only a subensemble of all oscillators is excited, resulting in a narrowband dip in the absorption spectrum (b)). Over time,spectral diffusion takes place, which leads to an increasingly shallower and broader dip in the absorption spectrum. c) The transient spectrum corresponding to b).

discuss the spectral diffusion of a mode which is induced by fluctuations of the site energies (δE). In case these fluctuations occur relatively slowly they lead to an inhomogeneously broadened spectrum. The presence of a strongly inhomogeous broadening mechanism can sometimes be directly inferred by linear spectroscopy, since in most cases, it leads to Gaussian lineshapes in contrast to Lorentian lineshapes for isolated (homogeneously broadened) vibrations. In general, it is not always possible to use the linear spectrum to determine which broadening mechanism is dominant since other close-by modes may obscure the lineshape or the inhomogeneity may be small relative to the natural linewidth.

In pump-probe spectroscopy this distinction is straightforward. Figure 2.12 demonstrates the principle of a hole-burning experiment where a narrowband pump pulse is used to excite a subband of an inhomogeneously broadened ensemble of oscillators. At short time delays, the pump will have bleached a relatively narrow hole into the absorption spectrum. With increasing pump-probe delay, all oscillators of the inhomogeneous distribution will interconvert, resulting in an increasingly broader and shallower hole. It is worth noting that the mere fact that one is able to bleach a hole in the absorption peak provides a direct confirmation that the transition in question is inhomogeneously broadened. In addition, the rate of the broadening (of the bleached hole) provides direct access to the timescale of the frequency fluctuations exhibited by the oscillators.

The frequency-frequency correlation function (FFCF) is proportional to the probability that an oscillator of a given frequency still has the same frequency after a certain period of time. Hence, by measuring the FFCF one can quantify the spectral diffusion of a given system. For an inhomogeneous ensemble of molecular vibrations, this can be achieved by performing a hole-burning experiment at different frequency positions within the corresponding absorption peak. In fact, if we stack all these hole-burning experiments on top of each other for a certain pump-probe delay we obtain a 2DIR spectrum. We can follow the spectral diffusion dynamics by monitoring the 2DIR lineshapes as a function of the pump-probe delay.

For short pump-probe delays all oscillators will be detected at the same frequency at which they were excited, resulting in diagonally elongated, elliptical 2DIR lineshapes
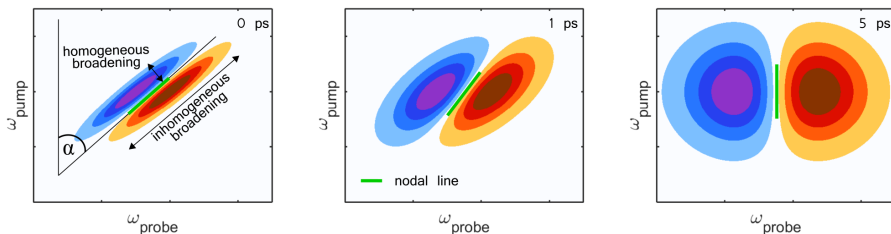
FIGURE 2.13. Measuring the inverse nodal line slope (INLS). All panels show the bleach (red) and ESA (blue) of a vibrational mode at different pump-probe delays. Directly after excitation, the diagonal width indicates the degree of inhomogeneous broadening and the anti-diagonal width the degree of homogeneous broadening. The anti-diagonal width increases with increasing time delay resulting in increasingly circular lineshapes and an increased slope of the nodal line (green).

(Fig. 2.13 left). With increasing delay time, the local environment of most oscillators will vary, which in turn changes their frequency. The frequency redistribution of the excited vibrations can be observed as the reshaping of the 2DIR lineshape with delay time (Fig. 2.13 right).

Similar to the previous section, we describe the frequency-frequency-correlation as $FFCF(t) = \langle \delta\omega(0)\delta\omega(t)\rangle$, where $\delta\omega$ denotes the instantaneous deviation from the fundamental transition frequency ω. Assuming random Gaussian fluctuations of the fundamental frequencies, it can be shown that to good approximation the FFCF decays exponentially:[73]

$$FFCF(t) = \langle \delta\omega(0)\delta\omega(t)\rangle = \Delta\omega^2 e^{-\frac{|t|}{\tau_c}}, \tag{2.93}$$

where τ_c is the decay constant of the correlation and $\Delta\omega$ the amplitude of the fluctuation.

There are various methods to extract the FFCF from the time-dependent 2DIR spectrum.[75,76] One of these methods uses the slope of the nodal line (green line in Figure 2.13) as it was shown that the inverse of this parameter is approximately proportional to the FFCF.[76] By plotting the decay of the inverse nodal line slope verses delay time one obtains the FFCF, which provides direct access to the timescale of the spectral diffusion. In general, however, the fluctuation of the vibrational frequency of a molecular vibration mostly result from the fast (orientational) motions of close-by solvent molecules (see Fig. 1.3). In Chapter 4, we will show how spectral diffusion measurements can yield insight into the solvent exposure of the amide groups of specific amino acids in peptides and proteins.